Crystal structure of human nicotinamide mononucleotide adenylyltransferase in complex with NMN

Erik Werner[a], Mathias Ziegler[b], Felicitas Lerner[b], Manfred Schweiger[b], Udo Heinemann[a,c,*]

[a] *Crystallography Group, Max Delbrück Center for Molecular Medicine, Robert-Rössle-Str. 10, D-13092 Berlin, Germany*
[b] *Institute of Chemistry – Biochemistry, Free University of Berlin, Thielallee 63, D-14195 Berlin, Germany*
[c] *Institute of Chemistry – Crystallography, Free University of Berlin, Takustr. 6, D-14195 Berlin, Germany*

Received 17 December 2001; revised 11 February 2002; accepted 28 February 2002

First published online 14 March 2002

Edited by Irmgard M. Sinning

Abstract The final step in the biosynthesis of nicotinamide-adenine dinucleotide, a major coenzyme in cellular redox reactions and involved in intracellular signaling, is catalyzed by the enzyme nicotinamide mononucleotide adenylyltransferase (NMNAT). The X-ray structure of human NMNAT in complex with nicotinamide mononucleotide was solved by the single-wavelength anomalous dispersion method at a resolution of 2.9 Å. Human NMNAT is a symmetric hexamer whose subunit is formed by a large six-stranded parallel β-sheet with helices on both sides. Human NMNAT displays a different oligomerization compared to the archaeal enzyme. The protein–nicotinamide mononucleotide interaction pattern provides insight into ligand binding in the human enzyme.

Key words: Nicotinamide mononucleotide adenylyltransferase; Nicotinamide-adenine dinucleotide biosynthesis; X-ray crystallography; Single-wavelength anomalous dispersion; Protein quaternary structure

1. Introduction

Nicotinamide-adenine dinucleotide (NAD^+) is an essential molecule in all cells as coenzyme of oxidoreductases. It also is an important constituent of several intracellular signaling pathways [1]. The final step in the biosynthesis of NAD^+, the transfer of the adenylyl moiety of ATP to nicotinamide mononucleotide (NMN), is catalyzed by nicotinamide mononucleotide adenylyltransferase (NMNAT; E.C. 2.7.7.1) [2]:

$$NMN + ATP \rightarrow NAD^+ + PP_i$$

Human NMNAT is a 32-kDa protein that has been purified from placenta [3] and as recombinant protein [4,5]. It is easily assayed by monitoring the reduction of NAD^+ by alcohol dehydrogenase [6].

NMNAT is thought to play an important role in regulating the cellular NAD^+ pool after episodes of increased DNA damage, since it has been described to be associated with poly(ADP-ribosyl) polymerase (PARP1) [7,8]. Among numerous other processes, PARP1 is part of the DNA base-excision repair system [9–11] and therefore may consume a considerable amount of cellular NAD^+ under conditions of genotoxic stress. NMNAT is down-regulated in tumor cells and has been proposed as a chemotherapeutical drug target for this reason [12–15].

Three structures of two archaeal NMNATs have been published, one from *Methanococcus jannaschii*, PDB code 1f9a, in complex with ATP [16] and two from *Methanobacterium thermoautotrophicum*, PDB codes 1ej2 and 1hyb, in complex with NAD^+ and NMN/SO_4^{2-}, respectively [17,18]. Both enzymes share extensive sequence (55%) and structural similarity (root-mean-square deviation (r.m.s.d.) 1.02 Å, calculated with Swiss PDB Viewer [19]). Apparently, ligand binding has no substantial effect on the overall protein conformation. However, sequence similarity to the human protein is very low: 15.5% (*M. jannaschii*) and 15.4% (*M. thermoautotrophicum*) [20]; all sequence identities calculated with the program ALIGN (GeneStream Server).

Recently published were a number of additional structures of nicotinamide/nicotinate mononucleotide adenylyltransferases, which are: human NMNAT apoenzyme, PDB code 1kku [21]; human NMNAT in complex with deamido-nicotinamide-adenine dinucleotide (NaAD), NAD and β-CH_2–tiazofurin adenine dinucleotide, PDB codes 1kqo, 1kqn and 1kr2, respectively [22]; *Escherichia coli* NaMNAT apoenzyme and complex with NaAD, PDB codes 1k4k and 1k4m, respectively [23]; *Bacillus subtilis* NaMNAT apoenzyme and complex with NaAD, PDB codes 1kam and 1kaq, respectively [24].

NMNAT is a member of the nucleotidyltransferase superfamily of α/β phosphodiesterases, proposed by Izard and Geerlof [25]. The related SCOP superfamily is the nucleotidylyltransferase superfamily [26]. Members include class I aminoacyl-tRNA synthetases (catalytic domain) [27], cytidyltransferase [28], ATP sulfurylase [29,30], and phosphopantetheine adenylyltransferase (PPAT) [25].

*Corresponding author. Fax: +49-30-9406-2548.
E-mail addresses: ewe@mdc-berlin.de (E. Werner), mziegler@chemie.fu-berlin.de (M. Ziegler), heinemann@mdc-berlin.de (U. Heinemann).

Abbreviations: NMNAT, nicotinamide mononucleotide adenylyltransferase; NaMNAT, nicotinate mononucleotide adenylyltransferase; NAD^+, nicotinamide-adenine dinucleotide; NMN, nicotinamide mononucleotide; NaAD, deamido-NAD; SAD, single-wavelength anomalous dispersion; NCS, non-crystallographic symmetry; SeMet, selenomethionine; r.m.s.d., root-mean-square deviation

0014-5793/02/$22.00
PII: S0014-5793(02)02556-5

2. Materials and methods

2.1. Expression, purification, crystallization, X-ray diffraction and data reduction

Expression of the human NMNAT cDNA in *E. coli* [4], purification of the protein and crystallization was performed as previously described [20]. The growth medium and conditions were modified according to a protocol of Van Duyne et al. [31] to produce protein that contains selenomethionine (SeMet) in place of methionine. A complete dataset at wavelength 0.9795 Å (peak of the fluorescence spectrum) was collected at beamline ID14-4, ESRF Grenoble, with reflections at a maximum resolution of 2.7 Å. Data were processed using DENZO and SCALEPACK [32].

2.2. Phase determination and refinement

Phases were determined with SOLVE [33] using only the peak dataset (maximal resolution used: 3.7 Å) and, therefore, the single-wavelength anomalous dispersion (SAD) method. Phases were improved by maximum-likelihood density modification, using RESOLVE [34] as well as non-crystallographic symmetry (NCS) averaging. For the latter, the three-fold NCS observed in the electron density was used in DM [35]. This program was also used for phase extension to 2.9 Å. The protein model was built by first placing a poly-alanine trace into the electron density of the peptide backbone and then mutating the residues according to the sequence of NMNAT (program ONO [36]). With the best selenium coordinates obtained this way, the phases were improved by re-running SOLVE, now omitting the NCS averaging by DM and using reflections up to 2.9 Å resolution, making phase extension by DM unnecessary. For refinement, the maximum-likelihood method as well as one simulated annealing step were used (programs REFMAC5 [35] and CNS [37], respectively). NCS restraints as well as *B*-factor restraints were held tight for the backbone and relaxed for the side-chain atoms during refinement.

3. Results and discussion

3.1. Purification, crystallization and structure determination

To produce SeMet-substituted NMNAT, recombinant *E. coli* cells were grown in a medium depleted of methionine, to which SeMet was added prior to induction. This way, SeMet was incorporated into NMNAT quantitatively. SeMet was detected by mass spectrometry. For example, the fragment Val67–Lys75 contained almost exclusively SeMet. SeMet substitution was also confirmed by a fluorescence scan prior to the diffraction experiment (data not shown). The crystallization conditions have been described elsewhere [20]. The enzyme activity remained unaffected by incorporating SeMet and was as previously described [4].

Phases yielding readily interpretable electron density were calculated with the SAD method. The number of nine sites in the Patterson map immediately indicated a three-fold symmetry of NMNAT which contains three internal methionines per subunit plus the N-terminal Met later found to be disordered. A trimer representing the asymmetric unit of the crystal was indeed seen in the electron density and used for NCS averaging. Despite this, the single monomers show some flexibility with respect to each other. The r.m.s.d. (calculated with the program LSQKAB [35]) between the monomers is 0.125/0.777 Å (main chain/all atoms) for monomers A and B, 0.131/0.850 Å for A and C, and 0.125/0.689 Å for B and C. The rotation angles are 119.16° between monomers A and B, 121.23° be-

Table 1
Data-collection and refinement statistics

Data collection	
Wavelength (Å)	0.9795
Resolution (Å)	20–2.9 (3.0–2.9)
No. of observations	632 186
Unique reflections	62 691 (5937)
Data completeness (%)	98.3 (92.5)
Average I/σ(I)	11.2 (1.1)
R^{a}_{merge} (%)	7.0 (49.2)
Space group	$C222_1$
Unit cell parameters (Å)	$a = 140.8$; $b = 235.7$; $c = 89.0$
Monomers in the asymmetric unit	3
Refinement	
Structure determination method	SAD
Se sites per asymmetric unit (no.)	9
Protein atoms (non-hydrogens) (no.)	5481
NMN atoms (non-hydrogens) (no.)	66
R^{b}_{cryst} (%)	25.3
R^{c}_{free} (%)	29.1
r.m.s.d. bond lengths (Å)	0.018
r.m.s.d. bond angles (degrees)	1.719
Average *B*-factor[d], all atoms (Å^2)	52.0
Average r.m.s.d. for mainchain *B*-factors[d] (Å)	1.35
Average r.m.s.d. for sidechain *B*-factors[d] (Å)	4.03

Values in parentheses refer to the outer resolution shell.
[a] $R_{merge} = \Sigma_{hkl}\ \Sigma_i |I_i - \langle I \rangle| / \Sigma \langle I \rangle$ where I_i is the intensity of the observation of reflection hkl, and $\langle I \rangle$ is the average intensity of this reflection.
[b] $R_{cryst} = \Sigma ||F_{obs}| - |F_{calc}|| / \Sigma |F_{obs}|$.
[c] R_{free} was calculated using 7% randomly selected reflections.
[d] Calculated with BAVERAGE [35].

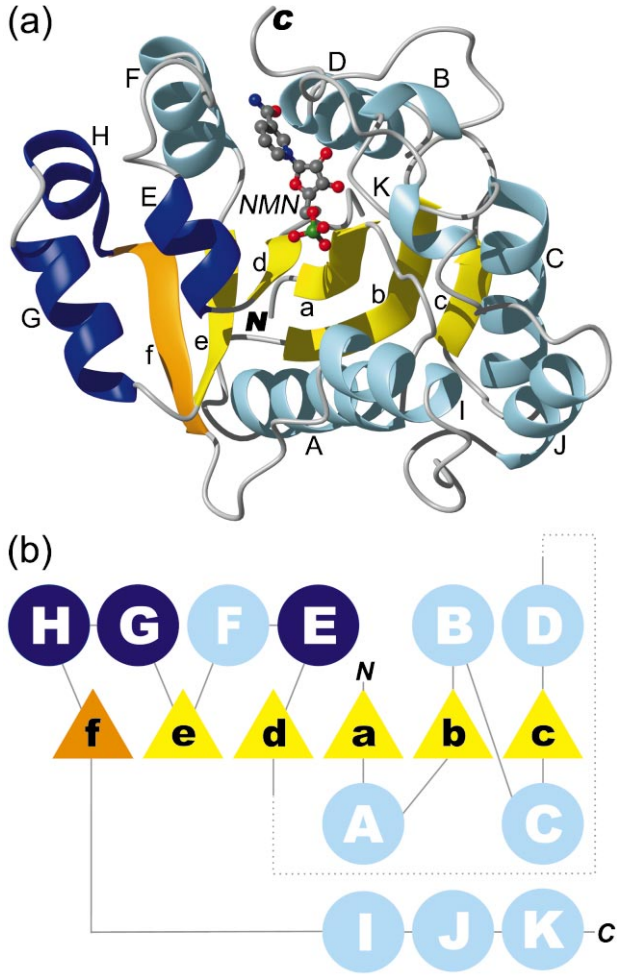

Fig. 1. Ribbon model (a) and topology diagram (b) of human NMNAT (PDB code 1gry) in complex with NMN. Strands are in yellow/orange, helices in light and dark blue; atom colors: C, gray; N, blue, O, red; P, green.

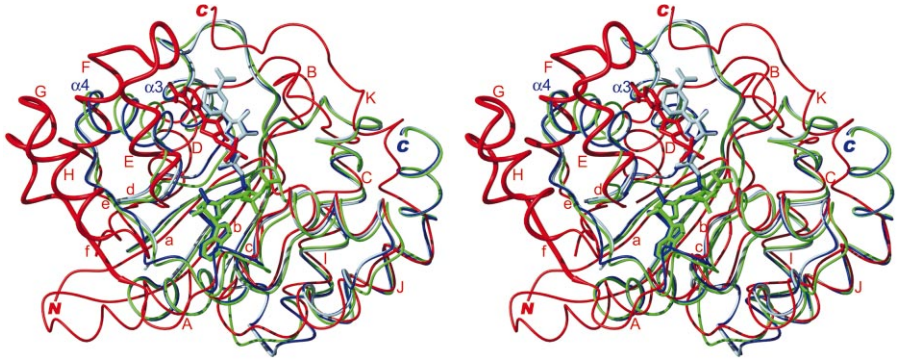

Fig. 2. Alignment of backbone atoms of human NMNAT (1gry, chain A, with NMN; red), *M. thermoautotrophicum* NMNAT (1ej2, with NAD^+; dark blue and 1hyb, with NMN; light blue) and *M. jannaschii* NMNAT (1f9a, chain A, with ATP; green). All proteins were aligned with 1ej2 as rigid chains. Helices E, F, G and H of 1gry, which are different or additional with respect to the archaeal enzymes, are shown with increased chain diameter.

tween A and C, yielding a slightly improper three-fold non-crystallographic axis. A crystallographic two-fold axis forms a hexamer with 32 point symmetry as biological unit. The electron density of the hexamer is clearly separated from solvent in the unit cell, and subunit contacts in the hexamer are much tighter than typical lattice contacts. In principle, but not in detail (see below), the quaternary structure of human NMNAT resembles that of two archaeal NMNATs [16,18]. Data collection and refinement statistics are given in Table 1.

3.2. Overall structure and oligomerization

The limited resolution of 2.9 Å, the relatively poor signal-to-noise in the high-resolution bins (reflections from 2.9 to 2.7 Å were not used) and the high average *B*-factor of the diffraction data permit a clear view of the global structure, but make it difficult to discuss fine structural details. The overall fold, the backbone and most side chains are well defined as well as a part of the ligand. Not seen in the electron density is a loop ranging from residues Leu106 to Lys146 as well as part of the ligand (see below). The missing loop, that is disordered in all three human structures (1KKU: residues 111–147 [21]; 1KYN: residues 109–146 [22]), contains a nuclear localization sequence, residues Pro123 to Trp129 [4] and is located at the outside of the biological hexamer (see Fig. 4a). Obviously, this part of the enzyme is highly flexible and accessible as indicated by the finding that trypsin cleaves human NMNAT preferentially at position Lys146 (data not shown).

The structure of human NMNAT consists of a large six-stranded parallel β-sheet that accounts for 16% of the sequence. On both sides, the sheet is covered by helices (40% of the structure), see Fig. 1 for a ribbon model of the (αβ-) structure (a) and a topology diagram (b). Overall conformational differences of the three human NMNAT structures are not obvious as judged from the published ribbon representations (coordinates are not available yet). For *E. coli*, NMNAT drastical conformational changes upon ligand binding were reported [23]. Structure and sequence of NMNAT from *M. thermoautotrophicum* (PDB codes 1ej2 (with NAD) and 1hyb (with NMN) [18]) and *M. jannaschii* (PDB code 1f9a (with ATP) [16] are very similar with respect to each other. Both do not show significant sequence similarity to the human enzyme: 15.5% identity to *M. jannaschii* NMNAT and 15.4% to *M. thermoautotrophicum* NMNAT after ClustalW alignment [20]). However, the structures share a common core. Compared to *M. thermoautotrophicum* NMNAT, the human enzyme contains approximately 50% more residues which account for additional secondary structure elements, highlighted in darker colors in Fig. 1a (dark blue for helices E, G and H; orange for strand f), and the missing loop from Leu106 to Lys146. See Fig. 2 for a structural alignment of the backbone of human and archaeal NMNATs. The Cα chains of the human and either one of the archaeal structures can be superimposed with an r.m.s.d. of 1.62 Å (calculated with Swiss PDB Viewer [19]).

Fig. 3 shows a sequence alignment, optimal with respect to the scoring function (sum-of-pairs alignment calculated with

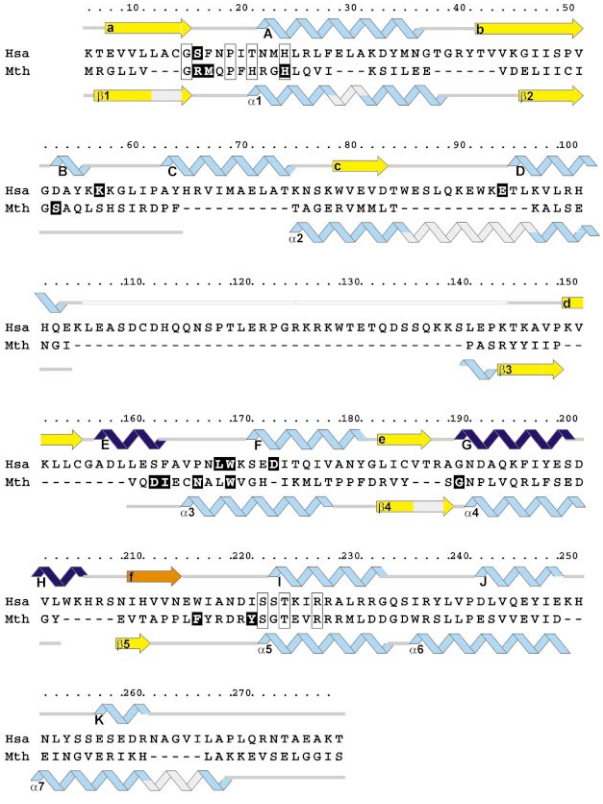

Fig. 3. Sequence alignment and associated secondary structure of human (Hsa) and *M. thermoautotrophicum* (Mth; numbering according to the original publication) NMNAT. Ligand-binding residues are highlighted in black boxes, the conserved residues of the conserved motifs GXXXPX(H/T)XXH and SXTXXR are framed; color code as in Fig. 1.

MSA [38]) of human and *M. thermoautotrophicum* NMNAT. Although the sequence similarity is weak, many secondary structure elements in fact do align. Helix F, which harbors or is near several of the ligand-binding residues is aligned with helix α3 of the archaeal NMNAT. However, a 3D-structure comparison (Fig. 2) shows that helix D of the human enzyme is the equivalent to this helix α3. This and the fact that NMN in the human enzyme is twisted compared to the ligand in the archaeal protein (see Figs. 2 and 5c) is a clear indication of a different cofactor binding behavior. Helix F, which together with helix E replaces *M. thermoautotrophicum* helix α4, is on the other side of that fork-like ligand-binding structural element.

The additional residues are also responsible for clear differences in the oligomerization of human NMNAT compared to the archaeal proteins (here shown and discussed for the *M. thermoautotrophicum* NMNAT [18]). This is hardly reflected in accessible surface area buried in the subunit interface (Fig. 4b) which, surprisingly, is almost identical for both proteins (approximately 2000 Å^2 per subunit; calculated with NACCESS [39], Fig. 4b). In the archaeal hexamer, the β-strands point towards the center of the hexamer, and the monomers sit squarely atop each other. In the human protein the monomers are oriented differently. The strands point more sideways and the monomers have extensive overlap to the adjacent monomers of the second-plane trimer (e.g. monomers A and D). The strands β3 (corresponding to the human strands d) of adjacent monomers A and E contact each other and are parallel in archaeal NMNAT. In human NMNAT, the opposite strands f (that have no correspondence in the archaeal proteins) do not contact directly, are antiparallel and formed by different monomers (A and D).

Fig. 4c shows details of the protein–protein interface in the human hexamer. Hydrogen bonds and hydrophobic contacts form a widespread net of interactions. In human NMNAT the dyad axis promotes interactions between helix A (residues 26–33; monomer A) and loop I–J (residues 234–237; monomer E) as well as, vice versa, loop I–J of monomer A and helix A of monomer E. Besides this, residues of monomer A contact those of monomer D. For example, a hydrogen bond between GlyA37 and ArgD207 is formed and a stacking of the aromatic rings of TyrA198 and TrpD216 is established. These contacts are repeated between momers B and D/F and between C and F/E. Within monomers related by the triad axis, residues 198–201 (helix G, monomer A) contact residues 228–232 (strand I, monomer B), which is regularly repeated between monomers B and C, C and A, D and E, E and F, and F and D. Most prominent are hydrogen bonds between Tyr198 and Arg232 and between Asp201 and Arg231, as well as a hydrophobic interaction between ArgA207, TrpA204 and ArgB232.

Triad axis interactions in the archaeal NMNAT are formed between helix α4 (corresponding to human helix F) of monomer A and helix α7 (corresponding to human loop J–K) of monomer B. This interaction is no longer possible in the human protein, because the additional helices G and H, lying right between them, drastically increase the distance between respective structural elements. Due to this changed overlap of adjacent trimer subunits, the lower trimer is forced to rotate with respect to the upper trimer where all monomers themselves are rotated compared to the archaeal hexamer arrangement.

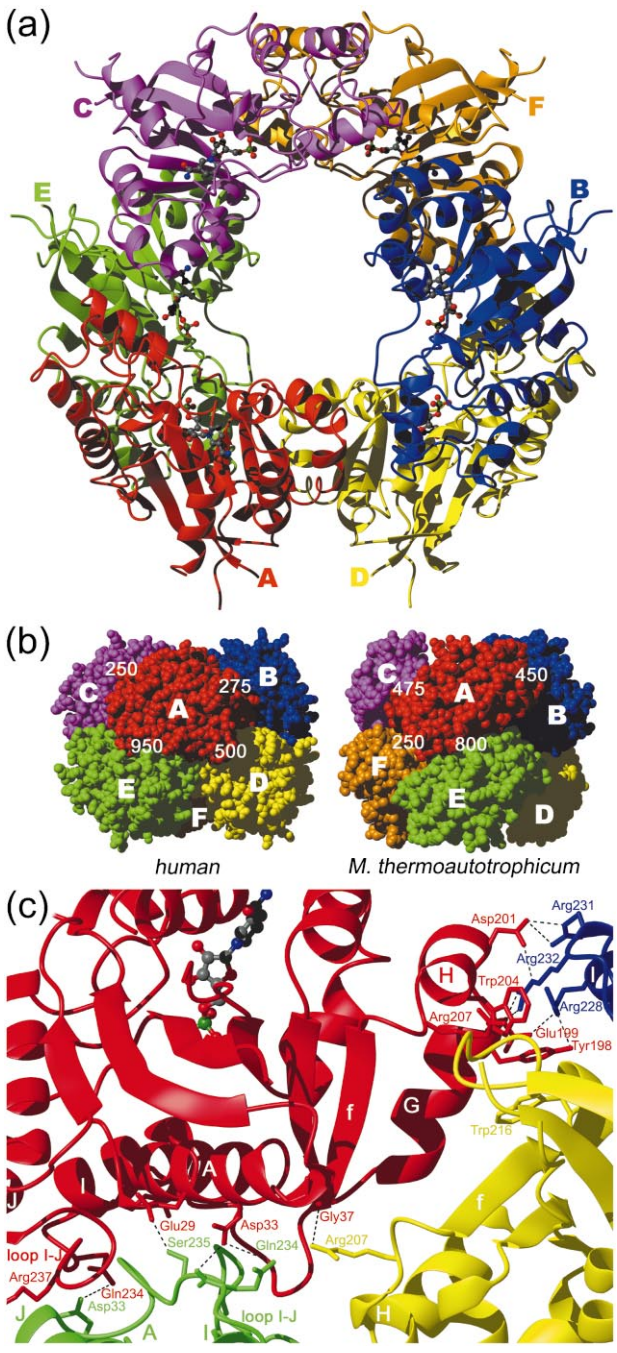

Fig. 4. Protein–protein interactions. a: Top view of the hexamer of human NMNAT with each subunit in a separate color (chain ID near the N-termini). Monomers A, B and C form the upper trimer, monomers D, E and F the lower trimer. b: Side view of human and *M. thermoautotrophicum* NMNAT in space-filling representation. Numbers represent the accessible surface area in Å^2 of subunit A buried in the subunit interface by the adjacent subunits. No contact is formed between monomers A and F in the human NMNAT or between A and D in the archaeal NMNAT. c: Contact area of human monomer A with its adjacent subunits B, D and E. Color code as in (b). Selected hydrogen bonds are shown as dotted lines, the label-color reflects the harvesting subunit. Subunits B, C and F are not shown.

The oligomerization of human NMNAT described here is in general consistent with the results of Garavaglia et al. [21] and Zhou et al. [22], although slight differences are reported (e.g. different hydrogen bonds for Tyr198). Since the structure described here has a leucine at position 217 (1KKU: Phe; a single nucleotide polymorphism [4]), the contact between regions 217–220 (loop f–I; monomer A) with the same region of monomer E is less intimate.

Bacterial NMNAT, in contrast to the hexameric archaeal and human proteins, is reported to occur in monomeric (*E. coli* [23]) or dimeric (*B. subtilis* [24]) forms.

3.3. Ligand binding

The crystallization buffer contained the cofactor NAD^+ at 1 mM concentration (1.6-fold molar excess with respect to the protein). In the electron density, only the NMN moiety of the ligand is seen. Although it cannot be excluded that the enzyme hydrolyzed NAD^+, it is more likely that the AMP or the adenosine part of NAD^+ is not revealed by the electron density due to positional flexibility. In fact, difference density is observed at a position where the second phosphate or the AMP ribose could be placed (Fig. 5b), close to His24, a potential ligand-binding residue and member of the highly conserved GXXXPX(T/H)XHXXH motif in all NMNAT sequences (see Fig. 3 and ref. [22]). *B*-factors of the ligand atoms are similar to those of nearby protein atoms, but slightly increased for the phosphate atoms, indicating a disordered adenylyl phosphate portion. An alternative possibility is that NMN was trapped in the protein during cell growth, as it was observed for the NMNAT structures of *M. thermoautotrophicum* [18]. However, since the AMP part is disordered or not present, this structure has to be discussed as a NMNAT–NMN complex.

The ligand-binding pocket faces the outer edges of the hexamer, being slightly tilted towards the central channel. The C-terminus may serve as a 'lock' of the cavity. NMN binding is achieved by hydrogen bonding and hydrophobic contacts of several amino acids of the binding pocket (Fig. 4, left). Most prominent are contacts of Ser16 and Lys57 with the phosphate oxygens and those of Glu94 to the nicotinamide and the ribose oxygens, as well as the stacking of Trp169 (conserved in all NMNAT sequences) with the nicotinamide. It has to be mentioned that within the three monomers in the asymmetric unit of the structure, the hydrogen bonding pattern is not strictly conserved. This could reflect flexibility of the binding pocket. For example the amido-nitrogen (N7) of NMN is hydrogen-bonded to the carbonyl oxygen of Leu168 (chain B) or to Asp173-OD1 (chain A). This binding-site flexibility is in line with the observation that NMNAT also catalyzes the synthesis of nicotinic acid adenine dinucleotide ($NaAD^+$) [40], see the discussion of NaAD binding to NMNAT [22].

Taking into account the limited resolution of our analysis and the observed binding-site flexibility, these results are in general agreement with the ligand-binding residues proposed for the NMNAT apoenzyme (1KKU) [21] and with the ligand-binding residues observed in the NMNAT–NAD^+ complex (1KQN) [22]. Two residues, however, are clearly different. In the apoenzyme, Glu94 is oriented away from the ligand-binding pocket whereas Trp92 is facing it. Here, Glu94 binds the ligand and the sidechain of Trp92 points away from the ligand (shortest distance of the ligand to

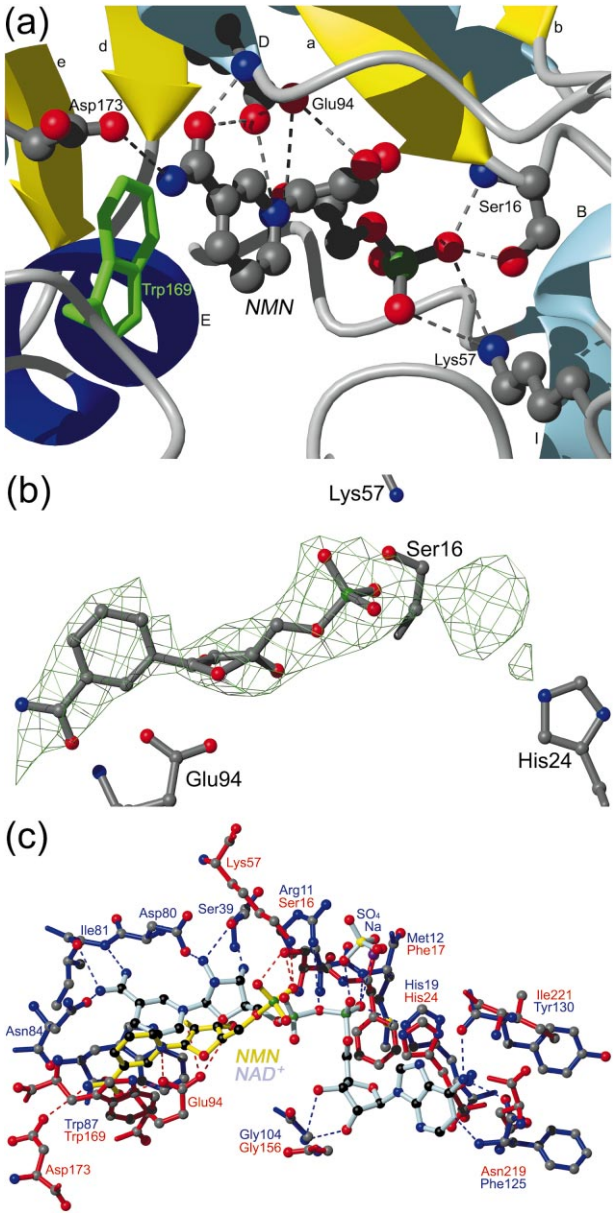

Fig. 5. Ligand-binding site of NMNAT. a: Human NMNAT binding NMN (chain A). Hydrogen bonds between protein residues and the ligand are shown as dotted lines, residue Trp169, stacking on the pyrimidine ring of NMN, is shown in green. Color code as in Fig. 1. b: *Fo–Fc* difference electron density map of the ligand-binding site (chain A). Calculated after refinement of the final model without the ligand, contoured with 2.5σ. Ball and stick representations of the ligand and adjacent amino acid side chains are shown. c: Ligand-binding site of human (1gry, chain A; amino acids in red, NMN in yellow) and *M. thermoautotrophicum* NMNAT (1ej2, amino acids in dark blue, NAD^+ in light blue) after alignment of the whole proteins. Hydrogen bonds between the protein residues and the ligand are shown as dotted lines in the respective color (1gry: red; 1ej2: blue).

Trp92 is 4.4 Å between the backbone carbonyl oxygen and the ribose oxygen O2R). In the NMNAT–NAD^+ complex, both residues participate in ligand binding. One could speculate that binding of NMN to the pocket is facilitated by a flip of the Glu94 sidechain and that Trp92 is part of an open–close system that is possibly connected to ATP binding.

Except for the stacking interaction of Trp169 (correspond-

ing to Trp87 in *M. thermoautotrophicum* NMNAT) and the possible hydrogen bonding of His24 (corresponding to *M. thermoautotrophicum* His19), only Ser16 is a conserved residue involved in ligand binding (see Figs. 3 and 5c). The tryptophans even belong to different regions of the proteins (loop E–F in human NMNAT, helix α3, corresponding to human helix D, in *M. thermoautotrophicum*). NMN in the human NMNAT structure presented here is rotated with respect to NAD^+ in *M. thermoautotrophicum* (Fig. 5c) and generally bound differently. Nevertheless, the active site and the ligand binding is to some extent similar in both structures of NMNAT, especially for the AMP part of the ligand. Although not matched by the sequence alignment, the AMP-binding residues Tyr130, Phe125 and Gly104 of *M. thermoautotrophicum* can be structurally related to human Ile221, Asn219 and Gly156 respectively (Fig. 5c). This is also true for PPAT for which a crystal structure in complex with dephospho-CoA is available (PDB code 1b6t [25]). In fact, PPAT gives the highest *Z*-score (13.8) in a DALI search [41] (*M. jannaschii* NMNAT, PDB code 1f9a, in second place with *Z*-score 11.6) and can be superimposed to the human NMNAT with a lower r.m.s.d. (1.41 Å) than the archaeal NMNATs.

4. Conclusion

The X-ray structure of the human NMNAT shows a globular (αβ) fold. The peptide stretch Leu106–Lys146, that contains the nuclear localization sequence and is not found in archaeal NMNATs, is located at the surface of the biological hexamer and not resolved in the structure due to disorder. Compared to the structures of two archaeal NMNATs, the human enzyme displays a different oligomerization, mediated by extra secondary structure elements. Three structures of human NMNAT, each recently published with a different ligand bound, reveal conformational differences of residues Glu94 and Trp92, that permit discussing a possible ligand-binding mechanism. The structure may help understand the role of human NMNAT in cellular signaling and permit to exploit the protein as a chemotherapeutical drug target.

5. Accession number

Coordinates of the structure of human NMNAT in complex with NMN have been deposited in the Protein Data Bank [42], PDB code 1gry.

Acknowledgements: We thank Klaus Hennig for excellent technical assistance, Eva Müller for mass spectrometric analyses, Uwe Mueller and the staff at ESRF Grenoble for help with data collection, and Yves A. Muller and Jürgen J. Müller for advice in crystallographic computing. E.W. gratefully acknowledges financial support from the Deutsche Forschungsgemeinschaft and the Fritz-Thyssen-Stiftung. This work is supported by the Deutsche Forschungsgemeinschaft (Schw 532/8-1) and the Fonds der Chemischen Industrie.

References

[1] Ziegler, M. (2000) Eur. J. Biochem. 257, 1550–1564.
[2] Magni, G., Amici, A., Emanuelli, M., Raffaelli, N., Ruggieri, S. (1999) in: Advances in Enzymology and Related Areas of Molecular Biology (Purich, D.L., Ed.), Vol. 73, pp. 135–160, John Wiley and Sons, New York.
[3] Emanuelli, M., Natalini, P., Raffaelli, N., Ruggieri, S., Vita, A. and Magni, G. (1992) Arch. Biochem. Biophys. 298, 29–34.
[4] Schweiger, M. et al. (2001) FEBS Lett. 492, 95–100.
[5] Emanuelli, M., Carnevali, F., Saccucci, F., Pierella, F., Amici, A., Raffaelli, N. and Magni, G. (2001) J. Biol. Chem. 276, 406–412.
[6] Balducci, E. et al. (1995) Anal. Biochem. 228, 64–68.
[7] Uhr, M.L. and Smulson, M. (1982) Eur. J. Biochem. 128, 435–443.
[8] Ruggieri, S., Gregori, L., Natalini, P., Vita, A., Emanuelli, M., Raffaelli, N. and Magni, G. (1990) Biochemistry 29, 2501–2506.
[9] Oei, S.L., Griesenbeck, J. and Schweiger, M. (1997) Rev. Physiol. Biochem. Pharmacol. 131, 127–174.
[10] D'Amours, D., Desnoyers, S., D'Silva, I. and Poirier, G.G. (1999) Biochem. J. 342, 249–268.
[11] Lindahl, T. and Wood, R.D. (1999) Science 286, 1897–1905.
[12] Emanuelli, M., Raffaelli, N., Amici, A., Balducci, E., Natalini, P., Ruggieri, S. and Magni, G. (1995) Biochem. Pharmacol. 49, 575–579.
[13] Hughes, K.T., Ladika, D., Roth, J.R. and Olivera, B.M. (1983) J. Bacteriol. 155, 213–222.
[14] Jayaram, H.N., Pillwein, K., Lui, M.S., Faderan, M.A. and Weber, G. (1986) Biochem. Pharmacol. 35, 587–593.
[15] Jayaram, H.N., Grusch, M., Cooney, D.A. and Krupitza, G. (1999) Curr. Med. Chem. 6, 561–574.
[16] D'Angelo, I., Raffaelli, N., Dabusti, V., Lorenzi, T., Magni, G. and Rizzi, M. (2000) Structure 8, 993–1004.
[17] Christendat, D. et al. (2000) Nat. Struct. Biol. 7, 903–909.
[18] Saridakis, V., Christendat, D., Kimber, M.S., Dharamsi, A., Edwards, A.M. and Pai, E.F. (2001) J. Biol. Chem. 276, 7225–7232.
[19] Guex, N. and Peitsch, M.C. (1997) Electrophoresis 18, 2714–2723.
[20] Werner, E., Ziegler, M., Lerner, F., Schweiger, M., Muller, Y.A. and Heinemann, U. (2002) Acta Crystallogr. Sect. 58, 140–142.
[21] Garavaglia, S., D'Angelo, I., Emanuelli, M., Carnevali, F., Pierella, F., Magni, G. and Rizzi, M. (2002) J. Biol. Chem. 277, 8524–8530.
[22] Zhou, T., Kurnasov, O., Tomchick, D.R., Binns, D.D., Grishin, N.V., Marquez, V.E., Osterman, A.L., Zhang, H. (2002) J. Biol. Chem. Pap. Press M111469200.
[23] Zhang, H., Zhou, T., Kurnasov, O., Cheek, S., Grishin, N.V. and Osterman, A. (2002) Structure 10, 69–79.
[24] Olland, A.M. et al. (2001) J. Biol. Chem. 277, 3698–3707.
[25] Izard, T. and Geerlof, A. (1990) EMBO J. 18, 2021–2030.
[26] Murzin, A.G., Brenner, S.E., Hubbard, T.J.P. and Chothia, C. (1995) J. Mol. Biol. 247, 536–540.
[27] Delarue, M. and Moras, D. (1993) BioEssays 15, 675–687.
[28] Weber, C.H., Park, Y.S., Sanker, S., Kent, C. and Ludwig, M.L. (1999) Structure 7, 1113–1124.
[29] Ullrich, T.C., Blaesse, M. and Huber, R. (2001) EMBO J. 20, 316–329.
[30] Ullrich, T.C. and Huber, R. (2001) J. Mol. Biol. 313, 1117–1125.
[31] VanDuyne, G.D., Standaert, R.F., Karplus, P.A., Schreiber, S.L. and Clardy, J. (1993) J. Mol. Biol. 229, 105–124.
[32] Otwinowski, Z. and Minor, W. (1997) Methods Enzymol. 276, 307–326.
[33] Terwilliger, T.C. and Berendzen, J. (1999) Acta Crystallogr. Sect. 55, 849–861.
[34] Terwilliger, T.C. (1999) Acta Crystallogr. Sect. 55, 1863–1871.
[35] Collaborative Computational Project, No. 4 (1994) Acta Crystallogr. Sect 50, 760–763.
[36] Jones, T.A., Zou, J.Y., Cowtan, S.W. and Kjeldgaard, M. (1991) Acta Crystallogr. Sect. 47, 110–119.
[37] Brünger, A.T. et al. (1998) Acta Crystallogr. Sect. 54, 905–921.
[38] Gupta, S.K., Kececioglu, J.D. and Schaffer, A.A. (1995) J. Comp. Biol. 2, 459–472.
[39] Hubbard, S.J., Thornton, J.M. (1993) NACCESS, computer program, Department of Biochemistry and Molecular Biology, University College London.
[40] Dahmen, W., Webb, B. and Preiss, J. (1967) Arch. Biochem. Biophys. 120, 440–450.
[41] Holm, L. and Sander, C. (1993) J. Mol. Biol. 233, 123–138.
[42] Berman, H.M., Westbrook, J., Feng, Z., Gilliland, G., Bhat, T.N., Weissig, H., Shindyalov, I.N. and Bourne, P.E. (2000) Nucleic Acids Res. 28, 235–242.